HHS Public Access

Author manuscript

J Vis Exp. Author manuscript; available in PMC 2020 April 30.

Determining Bile Duct Density in the Mouse Liver

Joshua M. Adams[1,2,3] and **Hamed Jafar-Nejad**[1,3]

[1]Program in Developmental Biology, Baylor College of Medicine, Houston, TX, USA

[2]Medical Scientist Training Program (MSTP), Baylor College of Medicine, Houston, TX, USA

[3]Department of Molecular and Human Genetics, Baylor College of Medicine, Houston, TX, USA

Abstract

Mouse is broadly used as a model organism to study biliary diseases. To evaluate the development and function of the biliary system, various techniques are used, including serum chemistry, histological analysis, and immunostaining for specific markers. Although these techniques can provide important information about the biliary system, they often do not present a full picture of bile duct (BD) developmental defects across the whole liver. This is in part due to the robust ability of the mouse liver to drain the bile even in animals with significant impairment in biliary development. Here we present a simple method to calculate the average number of BDs associated with each portal vein (PV) in sections covering all lobes of mutant/transgenic mice. In this method, livers are mounted and sectioned in a stereotypic manner to facilitate comparison among various genotypes and experimental conditions. BDs are identified via light microscopy of cytokeratin-stained cholangiocytes, and then counted and divided by the total number of PVs present in liver section. As an example, we show how this method can clearly distinguish between wild-type mice and a mouse model of Alagille syndrome. The method presented here cannot substitute for techniques that visualize the three-dimensional structure of the biliary tree. However, it offers an easy and direct way to quantitatively assess BD development and the degree of ductular reaction formation in mice.

SUMMARY:

We present a rather simple and sensitive method for accurate quantification of bile duct density in the mouse liver. This method can aid in determining the effects of genetic and environmental modifiers and the effectiveness of potential therapies in mouse models of biliary diseases.

Keywords

liver development; bile duct; cytokeratin; Notch signaling; Alagille syndrome; *Jag1*

Corresponding Author: Hamed Jafar-Nejad, hamedj@bcm.edu.

DISCLOSURES:
The authors have no conflict of interest.

INTRODUCTION:

The biliary tree is a critical part of the mammalian liver, allowing the passage of bile from hepatocytes into the gut. Intrahepatic bile ducts (BDs) are formed by cholangiocytes, which differentiate from bipotential hepatoblasts through Notch and TGFβ signaling[1,2]. Proper specification and commitment of cholangiocytes and their assembly into mature BDs are critical for the development of the intrahepatic biliary tree. As the liver grows during development or upon organ regeneration, the biliary system needs to develop along the liver to ensure proper bile drainage. Moreover, a number of syndromic and non-syndromic diseases result in the paucity of intrahepatic BDs[3]. In addition, a number of acute and chronic liver diseases give rise to so-called ductular reactions in the liver, which are defined as the presence of a significant number of cells that express biliary markers but do not necessarily arise from biliary cells or form patent BDs[4]. In the multisystem disorder Alagille syndrome (ALGS), haploinsufficiency of the Notch ligand jagged1 (*JAG1*) results in poor BD formation and cholestasis[5,6]. Our lab recently demonstrated that a previously generated *Jag1* heterozygous mouse line[7] is an animal model of BD paucity in ALGS[8]. In this mouse model of ALGS, cholangiocytes are still present. However, they fail to commit to incorporation into mature, patent BDs[8]. Therefore, analysis of the liver in a model of BD paucity requires more than the apparent presence or absence of cholangiocytes. It is important to accurately assess the degree to which mature BDs are present in the liver.

In anatomic pathology, there are accepted quantitative methods for assessing whether BD paucity exists[9]. For example, studies on ALGS in human patients often quantify the BD to portal vein (PV) ratio by analyzing at least 10 PVs per liver biopsy[9,10]. Analysis of the shape and overall presence or absence of patent BDs, combined with serum chemistry, can provide valuable information about BD development in mice[11–13]. However, mice can lose a significant number of BDs with only a modest increase in serum bilirubin level[8]. Accordingly, a quantitative method that evaluates the number of BDs present per PV can provide a more direct measure of the degree of BD paucity in mice. In a recent report, we quantified the number of BDs per PV across all liver lobes and reported a significant decrease in the BD to PV ratio in *Jag1+/−* animals[8]. During the course of our analysis, we noticed that despite the significant variation in the degree of inflammatory response and ductular reactions, the BD to PV ratio does not show much variability[8]. Moreover, quantification of the BD to PV ratio allowed us to demonstrate that removing one copy of the glycosyltransferase gene *Poglut1* in *Jag1+/−* animals can significantly improve their BD paucity[8]. In a *Jag1+/+* background, conditional loss of *Poglut1* in vascular smooth muscle cells results in a progressive increase in BD numbers, which is modest (20–30%) at P7 but becomes prominent in adults[8]. Again, this technique allowed us to show that even at P7, the increase in BD density in these animals is statistically significant. Of note, the increased BD density in this genotype at four months of age was validated through resin cast analysis as well.[8] These observations and other reports which measured BD density in different ALGS mouse models[14,15] prompted us to incorporate this method into our overall strategy to analyze biliary defects in various mutant and transgenic mice.

Here, we detail a straightforward technique which can be used to examine the degree of BD paucity in mouse models of liver disease (Figure 1). In this method, co-staining with

cholangiocyte markers cytokeratin (CK) 8 and CK19 (hereafter wide-spectrum CK, wsCK) is used to visualize BDs and unincorporated cholangiocytes in the mouse liver. An antibody against alpha-smooth muscle actin (αSMA) is added to the staining to label vessels. Systematic analysis of the BD to PV ratio in a section covering all liver lobes ensures that a large number of PVs are analyzed for each genotype. Since our method relies on quantifying BDs and PVs in 2D images, it is not suitable for studying the effects of a given mutation on the 3D structure of the biliary tree or the integrity of the small biliary conduits. Nevertheless, it provides a simple and objective strategy for investigators to assess biliary development in the mouse.

PROTOCOL:

All animals were housed in a barrier animal facility at Baylor College of Medicine per Institutional Animal Care and Use Committee guidelines and under approved animal protocols.

1. Collection of mouse liver tissue

1.1. Preparation of mouse for liver harvest

1. Euthanize the mouse using isoflurane.
2. Perform cervical dislocation of the mouse to ensure death.
3. Make a transverse incision approximately one inch below the rib cage.
4. Expose the entire ventral surface of the liver.

1.2. Collection of the mouse liver

1. Carefully, with small scissors, cut through the ligaments connecting the liver to other organs in the abdomen.
2. Cut through the common BD to detach the liver from the intestine.
3. Carefully remove the liver by holding onto the gallbladder and immediately place in a 50 mL tube filled to three-quarters by 4% paraformaldehyde (PFA).

2. Fixation and embedding the liver in paraffin

2.1. Fixation

1. Fix the liver tissue for 48 h in 4% PFA at 4 °C.
2. Wash the tissue with 70% EtOH for 1 h at 4 °C.
3. Wash the tissue twice with 95% EtOH for 1 h each at 4 °C.
4. Wash the tissue twice with 100% EtOH for 1 h each at 4 °C.

2.2. Clearing

1. Wash the liver tissue with clearing agent (Table of Materials) three times for 30 min each at room temperature.

NOTE: The liver should feel rigid following the third wash.

2.3. Embedding in paraffin

1. Place the tissue cassette in a tissue mold in paraffin wax for 3 washes, 30 min each. Wax should be preheated to 60 °C.
2. Fill the tissue mold with paraffin wax to three-quarters height and keep on a heating block at 60 °C.
3. Place the liver in the mold with the ventral side facing up.
4. Carefully remove the mold from the heating block.
5. Place the top of the cassette on the mold and top off with hot liquid paraffin.
6. Allow the mold and block to cool to room temperature overnight.

   NOTE: Tissue blocks can now be stored at room temperature.

3. Sectioning liver tissue

3.1. Preparation of the block for sectioning

1. Place the mold on ice for 5 min before removing the block from the mold.
2. Place the block on ice with a lab tissue paper present between block and ice.
3. Keep the block on ice when not sectioning for best tissue slicing results.

3.2. Sectioning the liver blocks

1. Using a microtome, begin by sectioning through the superficial, dorsal side of the liver. Sections should be 5 μm.
2. Check the superficial sections under a dissection microscope to ensure sections are not sheared or folded.
3. Take a section of the liver that includes the caudate lobe.

   NOTE: For some blocks, you will have the left, medial, right and caudate lobes on the same tissue slice.
4. For those blocks where all four lobes are not present on the same slide, continue to slice until the left, medial and right lobes are present on the same slide.

4. Immunohistochemistry for wsCK and αSMA

4.1. Processing of slides for immunohistochemistry

1. Select one slide per genotype to be analyzed.
2. Wash the slide for 15 min in Xylene, 100% EtOH, 95% EtOH and finally 70% EtOH (3 × 5 min in each solution).
3. Wash the slide for 5 min in deionized H_2O.
4. Immerse the slide in the antigen retrieval solution (Tris-based, high pH).

5. Heat under pressure in a pressure cooker for 3 min at 10 psi.
6. Allow the slide to cool to room temperature (approximately 35 min).

4.2. Blocking the tissue sections

1. Using a Pap Pen, outline the sections on the slide.
2. Apply phosphate-buffered saline (PBS) + 0.1% Tween to cover the section twice, 5 min each.
3. Make blocking buffer by mixing Normal Goat Serum (NGS) at 1:50 in PBS + 0.3% Triton. To have enough buffer for both blocking and primary antibody application, 100 µL per section is sufficient.
4. Apply 100 µL of blocking solution per section.
5. Incubate the slides covered with the blocking solution at 4 °C for 1 h.

4.3. Staining for wsCK and αSMA

1. Dilute anti-CK8 and anti-CK19 antibodies[16] (Developmental Studies Hybridoma Bank, TROMA-I and TROMA-III, respectively) 1:20 in blocking buffer to stain for wsCK. Dilute the anti-αSMA antibody[17] (Table of Materials) to 1:200 in the same buffer.
2. Apply 100 µL of the diluted antibody solution containing all three antibodies to each section.
3. Incubate the slides covered with the antibody solution at 4 °C overnight.
4. Wash the slides with PBS + 0.1% Triton three times, 5 min each.
5. Dilute secondary antibodies (anti-rat-Alexa488 and anti-mouse-Cy5) 1:200 in PBS + 0.3% Triton.
6. Apply 100 µL of the secondary antibody solution containing both secondary antibodies to the slides.
7. Incubate at room temperature for 1 h.

4.4. DAPI nuclear staining and mounting

1. Wash the slides three times, 5 min each.
2. Apply 100 µL of DAPI (1:3000) to each section for 10 m.
3. Apply Antifade Mounting Medium (Table of Materials) to the slides and place a glass coverslip on top of the tissue sections. Leave the slides at 4 °C overnight. Seal the slides the next day.
4. Store the slides at 4 °C and image within 1 week of mounting.

5. Imaging and quantification of BDs

5.1. Imaging liver sections

1. rior to imaging, blind yourself to the genotype of the sample with help from a lab member. Ensure all imaging files are devoid of genotype or other specific identifying information besides an animal/sample number.
2. Using a fluorescent microscope, take 20X images at 1X zoom of each section and ensure that every PV across the liver is imaged. Include the left, medial, right and caudate lobes.

   NOTE: We usually find 60–90 portal tracts per animal depending on the size of the liver.
3. To identity the PVs, look for αSMA plus wsCK staining. Structures that are αSMA positive but lack wsCK staining are not portal structures.

5.2. Identification and counting of BDs

1. Create a spreadsheet with the following columns: Animal/Sample Number, Image Number, Number of PVs and Number of BDs.
2. Going through each image, identify and record the number of PVs per image.
3. Identify patent BDs in each image by the presence of cholangiocytes (wsCK+) surrounding a definable lumen. Structures should be distinct and separated by mesenchyme from other wsCK+ cells.
4. Count each patent BD and place in the same column as the image number.
5. Do this for each image taken of a PV.
6. Calculate the sum of all PVs and all BDs in the liver sample.
7. Calculate the BD to PV ratio for the liver sample.

REPRESENTATIVE RESULTS:

We previously documented biliary defects in *Jag1+/−* animals, a mouse model of ALGS[8]. To determine the BD to PV ratio, we sectioned P30 mouse livers and co-stained them for CK8 and CK19 (wsCK) along with the vascular marker αSMA. We then imaged all the PVs in each of the liver lobes. As shown in Figure 2A, we defined PVs as αSMA-stained vessels that have adjacent wsCK staining (arrowheads). The αSMA-stained structures without wsCK were central veins and should not be included in the analysis (arrow).

Once PVs were identified, we identified patent BDs by their characteristic shape. As shown in Figure 3, patent ducts have a clearly definable lumen that is surrounded by wsCK+ cholangiocytes. The ducts are usually separated from nearby ducts or cholangiocytes by mesenchyme (arrowhead). wsCK+ cells that do not have a definable lumen, are attached to adjacent cells, or appear in isolation, are not counted toward the total number of BDs (arrows). Figure 3A shows a wild-type liver section with a PV which is associated with a fully patent duct along with several unincorporated cells. Figure 3B is a representative liver

section from a P30 *Jag1+/−* animal. No patent BDs are present around the three PVs in this section. All wsCK+ cells are unincorporated and therefore should not be counted. This image highlights the importance of careful BD counting, as presence or absence of wsCK+ cells does not differentiate the *Jag1+/−* and wild-type livers.

As demonstrated in Figure 1D, analysis of the BD to PV ratio involves counting every PV in the liver section along with the total number of patent BDs present around each PV. While analyzing the *Jag1+/−* livers, we noticed that different lobes are not necessarily affected to the same extent in these animals (unpublished data). Therefore, we usually count PVs across the left, medial, right and caudate lobes to ensure complete liver coverage. Following tabulation of total PVs and BDs, the ratio is calculated for the whole section.

In Figure 4, we showed the analysis of the BD to PV ratios for 3 wild-type and 3 *Jag1+/−* animals. This graph shows how the two genotypes can be readily distinguished based on BD counts. Additionally, this method provides a quantitative measure for analysis of the degree of rescue of the *Jag1+/−* phenotype by genetic manipulations, as reported previously[8].

DISCUSSION:

Analysis of BD development and repair in mice is an important tool in studying the pathogenesis and mechanism of cholestatic disorders. In addition, development of new therapies is in part dependent upon establishing a reproducible and preferably quantifiable phenotype. Current phenotyping in mouse models usually involves serum chemistry, liver histology and immunostaining for cell-type specific markers. Although these techniques generate valuable information about the structure and function of the biliary system, they do not provide a direct measure of the effects of a given genetic manipulation on the number of BDs. In anatomic pathology, BD paucity in human patients is determined through the analysis of BD to PV ratio in a biopsy section[9]. While clinicians employ serum chemistry analysis to determine the severity of cholestasis and liver disease in ALGS and other cholestatic diseases[18,19], histological assessment in mouse models is critical to both understanding the effects of disease modifiers on BD development and the effectiveness of therapies on restoring normal duct development. This is in part because mice can have a severe decrease in the number of patent BDs but still show only a modest increase in the serum bilirubin level[8], likely due to the highly efficient bile drainage in the mouse liver. Our previous work has shown that *Jag1* heterozygosity results in impaired BD maturation but not the absence of cholangcioytes[8]. Thus, to analyze BD development and assess disease severity in mouse models, it is not sufficient to merely examine the absence or presence of cholangiocytes. To address this issue, here we have presented a simple method for objective measurement of patent BD numbers in the mouse liver.

Our analysis is dependent on proper fixation and embedding of the mouse liver. Livers are embedded ventral side up to ensure similar sectioning from one sample to another. This is the most stable position. The sections used for staining must be deep enough in the liver lobes, as there are differences in the number of BDs and the size of PVs in the periphery versus the hilum of the liver. We occasionally see PVs that are cut longitudinally. In those cases, there is usually a neighboring BD that is also cut longitudinally and appears like a

long open tube. To ensure reproducibility, we count these long tubes as a single BD. Identification of patent BDs is unambiguous for the most part. However, some biliary structures appear lumenized but do not show the round to ellipsoid morphology typically seen in normal BDs[14]. In our hands, this can sometimes result in one structure being called a BD by an investigator but not by another colleague. Therefore, to ensure consistency and reproducibility in data analysis and presentation, we recommend that all samples related to a specific project be analyzed by two investigators independently.

Anti-CK8 has been shown to mark immature and mature biliary cells, while anti-CK19 only marks mature biliary cells[12,20]. Therefore, even if a PV is not associated with a mature BD, it can be readily differentiated from central veins because of the presence of CK8+ cells. Using these two antibodies in combination with anti-αSMA ensures complete coverage of portal tracts in our quantification. Moreover, in our hands, the individual CK19 or CK8 staining of the biliary cells generates a relatively weak signal and is associated with some background staining. Mixing the two CK antibodies results in a consistently strong signal in biliary cells and therefore facilitates the quantification.

Maturation of the intrahepatic biliary tree occurs in a hilar-to-peripheral direction and continues postnatally[21]. Indeed, there are many more immature cholangiocytes in early postnatal livers, especially in peripheral areas, which are at the leading front of postnatal liver expansion. Moreover, we observed a change in BD numbers as the animals age[8], with more ducts in older animals. In addition, some portal structures contain multiple BDs while others have one or no ducts, particularly along the liver periphery. We use a microscopy slide covering all liver lobes for each animal and systematically quantify the BD to PV ratio across the whole slide. While this is not essential, it ensures that ample portal tracts are analyzed for each animal regardless of age and liver size (60–90 PVs per liver depending on the genotype and age). Moreover, by analyzing all PVs on the slide, we ensure that both more mature hilar and less mature peripheral areas are counted at all stages of liver development. Covering all liver lobes for each animal can also decrease variability in measurements if a given mutation does not affect BD development uniformly across the liver.

The method is limited in distinguishing smaller bile conduits from groups of unincorporated biliary cells. The bile ductules[4] are usually too small to be recognized as a lumenized structure in the magnification that we use to analyze these stainings. Therefore, they are likely to be excluded from our quantifications, and thus the method is skewed towards identifying medium to large ducts. Despite this limitation, the method described here readily distinguishes between the *Jag1+/−* and *Jag1+/+* livers. Moreover, it is sensitive enough to detect the partial rescue of the *Jag1+/−* BD paucity upon simultaneous loss of one copy of *Polgut1+/−* and the modest increase in BD density in *Jag1+/+* animals with conditional loss of *Poglut1* in vascular smooth muscle cells[8]. These observations indicate this method's usefulness in determining alterations in BD density in various genetic backgrounds, even when the changes in BD number are modest.

In recent years, visualization of the 3D structure of the biliary tree has been used by several groups to analyze BD development[22–25]. These elegant methods rely on filling the biliary

tree from the common BD by ink or resin, and therefore examine the patency of the biliary system. Moreover, they provide information about the 3D structure of the biliary tree and its formation in the liver periphery as the liver grows, which cannot be assessed by 2D assessment used in protocols like the one presented here. However, successful performance of these 3D visualization techniques requires considerable expertise[26]. In contrast, the technique presented here is rather straightforward and can be executed by any group with access to routine equipment for histological and imaging analysis. Moreover, analysis of the sections double-stained for wsCK and αSMA will also show whether ductular reactions or vascular smooth muscle cell abnormalities exist in the liver[8,27,28]. We suggest that quantifying the BD to PV ratio in the whole liver sections can provide a sensitive and reproducible measure of biliary development in mice and can serve as a relatively easy technique to help the investigators decide whether they should consider more sophisticated techniques like 3D visualization of the biliary tree.

ACKNOWLEDGMENTS:

The authors acknowledge support from the National Institutes of Health (NIH) (R01 GM084135 and R01 DK109982), a Pilot/Feasibility Award from the Texas Medical Center Digestive Disease Center under NIH P30 DK56338, and an Alagille Syndrome Accelerator Award from The Medical Foundation.

REFERENCES:

1. Zong Y et al. Notch signaling controls liver development by regulating biliary differentiation. Development 136 (10), 1727–1739 (2009). [PubMed: 19369401]
2. Clotman F et al. Control of liver cell fate decision by a gradient of TGFβ signaling modulated by Onecut transcription factors. Genes & Development 19 (16), 1849–1854 (2005). [PubMed: 16103213]
3. Karpen SJ Update on the etiologies and management of neonatal cholestasis. Clin Perinatol 29 (1), 159–180 (2002). [PubMed: 11917736]
4. Roskams TA et al. Nomenclature of the finer branches of the biliary tree: canals, ductules, and ductular reactions in human livers. Hepatology 39 (6), 1739–1745 (2004). [PubMed: 15185318]
5. Oda T et al. Mutations in the human Jagged1 gene are responsible for Alagille syndrome. Nature Genetics 16 (3), 235 (1997). [PubMed: 9207787]
6. Li L et al. Alagille syndrome is caused by mutations in human Jagged1, which encodes a ligand for Notch1. Nature Genetics 16 (3), 243 (1997). [PubMed: 9207788]
7. Xue Y et al. Embryonic lethality and vascular defects in mice lacking the Notch ligand Jagged1. Human Molecular Genetics 8 (5), 723–730 (1999). [PubMed: 10196361]
8. Thakurdas SM et al. Jagged1 heterozygosity in mice results in a congenital cholangiopathy which is reversed by concomitant deletion of one copy of Poglut1 (Rumi). Hepatology 63 (2), 550–565 (2016). [PubMed: 26235536]
9. Hadchouel M Paucity of interlobular bile ducts. Seminars in Diagnostic Pathology 9 (1), 24–30 (1992). [PubMed: 1561486]
10. Emerick KM et al. Features of Alagille syndrome in 92 patients: frequency and relation to prognosis. Hepatology 29 (3), 822–829 (1999). [PubMed: 10051485]
11. Poncy A et al. Transcription factors SOX4 and SOX9 cooperatively control development of bile ducts. Dev Biol 404 (2), 136–148 (2015). [PubMed: 26033091]
12. Hofmann JJ et al. Jagged1 in the portal vein mesenchyme regulates intrahepatic bile duct development: insights into Alagille syndrome. Development 137 (23), 4061–4072 (2010). [PubMed: 21062863]

13. McCright B, Lozier J & Gridley T A mouse model of Alagille syndrome: Notch2 as a genetic modifier of Jag1 haploinsufficiency. Development 129 (4), 1075–1082 (2002). [PubMed: 11861489]
14. Andersson ER et al. Mouse Model of Alagille Syndrome and Mechanisms of Jagged1 Missense Mutations. Gastroenterology 154 (4), 1080–1095 (2018). [PubMed: 29162437]
15. Loomes KM et al. Bile duct proliferation in liver-specific Jag1 conditional knockout mice: effects of gene dosage. Hepatology 45 (2), 323–330 (2007). [PubMed: 17366661]
16. Brulet P, Babinet C, Kemler R & Jacob F Monoclonal antibodies against trophectoderm-specific markers during mouse blastocyst formation. Proc Natl Acad Sci U S A 77 (7), 4113–4117 (1980). [PubMed: 6933460]
17. Skalli O et al. A monoclonal antibody against alpha-smooth muscle actin: a new probe for smooth muscle differentiation. J Cell Biol 103 (6 Pt 2), 2787–2796 (1986). [PubMed: 3539945]
18. Kamath BM et al. A longitudinal study to identify laboratory predictors of liver disease outcome in Alagille syndrome. Journal of Pediatric Gastroenterology and Nutrition 50 (5), 526 (2010). [PubMed: 20421762]
19. Mouzaki M et al. Early life predictive markers of liver disease outcome in an International, Multicentre Cohort of children with Alagille syndrome. Liver International 36 (5), 755–760 (2016). [PubMed: 26201540]
20. Shiojiri N Development and differentiation of bile ducts in the mammalian liver. Microsc Res Tech 39 (4), 328–335 (1997). [PubMed: 9407543]
21. Crawford JM Development of the intrahepatic biliary tree. Semin Liver Dis 22 (3), 213–226 (2002). [PubMed: 12360416]
22. Kaneko K, Kamimoto K, Miyajima A & Itoh T Adaptive remodeling of the biliary architecture underlies liver homeostasis. Hepatology 61 (6), 2056–2066 (2015). [PubMed: 25572923]
23. Schaub JR et al. De novo formation of the biliary system by TGFbeta-mediated hepatocyte transdifferentiation. Nature 557 (7704), 247–251 (2018). [PubMed: 29720662]
24. Sparks EE, Huppert KA, Brown MA, Washington MK & Huppert SS Notch signaling regulates formation of the three-dimensional architecture of intrahepatic bile ducts in mice. Hepatology 51 (4), 1391–1400 (2010). [PubMed: 20069650]
25. Tanimizu N et al. Intrahepatic bile ducts are developed through formation of homogeneous continuous luminal network and its dynamic rearrangement in mice. Hepatology 64 (1), 175–188 (2016). [PubMed: 26926046]
26. Walter TJ, Sparks EE & Huppert SS 3-dimensional resin casting and imaging of mouse portal vein or intrahepatic bile duct system. J Vis Exp (68), e4272 (2012). [PubMed: 23128398]
27. Popper H, Kent G & Stein R Ductular cell reaction in the liver in hepatic injury. J Mt Sinai Hosp N Y 24 (5), 551–556 (1957). [PubMed: 13476145]
28. Yimlamai D et al. Hippo pathway activity influences liver cell fate. Cell 157 (6), 1324–1338 (2014). [PubMed: 24906150]

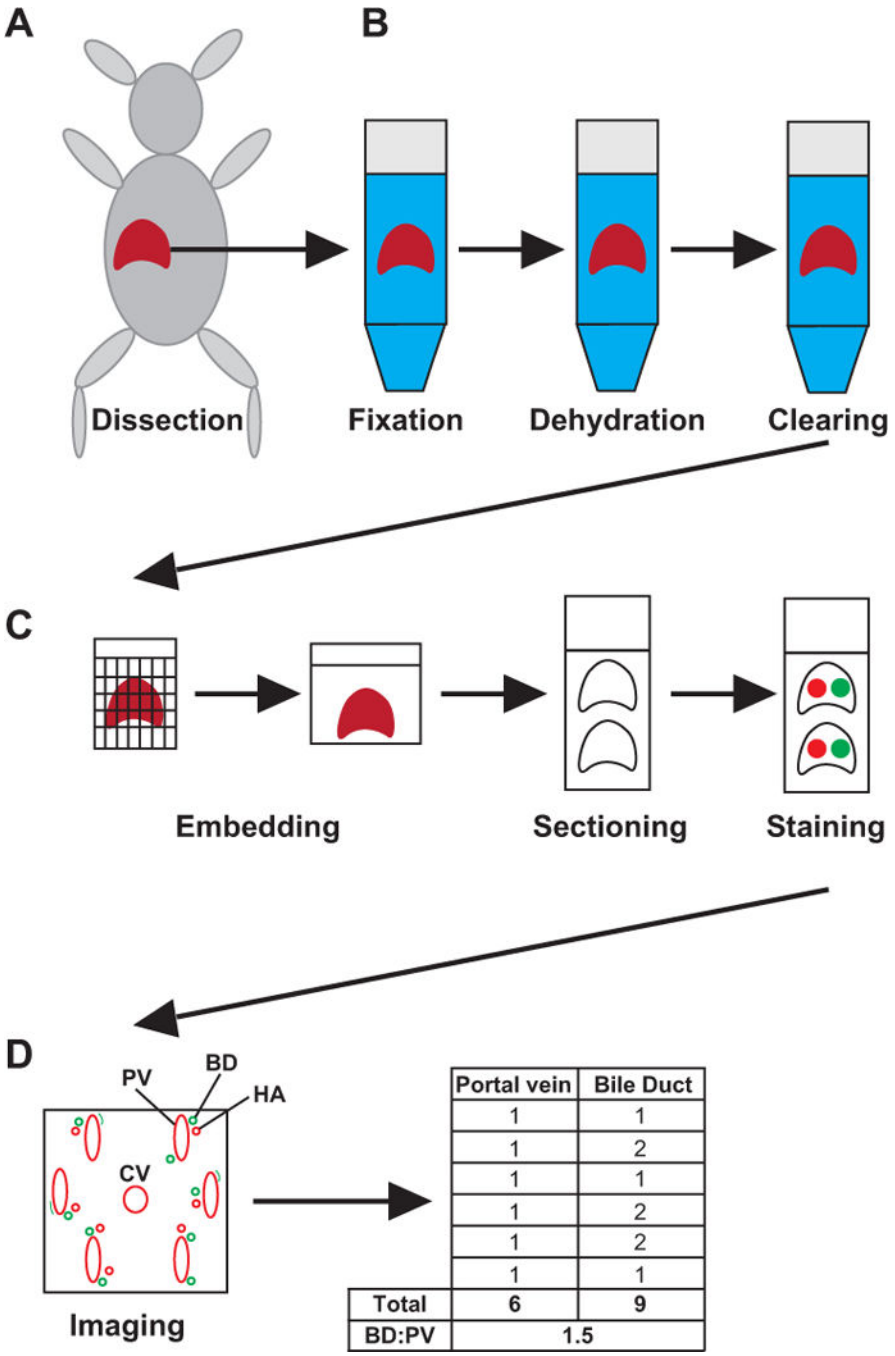

Figure 1. Schematic of the experimental process.

(A). The liver is harvested whole from the mouse. **(B).** Liver samples are fixed for 48 h, dehydrated and cleared. **(C).** The liver tissue is embedded in paraffin. Sections are made and placed on charged slides and stained for wsCK and αSMA. **(D).** Slides are imaged, and the number of PVs and BDs are recorded. The BD to PV ratio (BD:PV) is calculated for the entire liver section. HA, hepatic artery; CV, central vein.

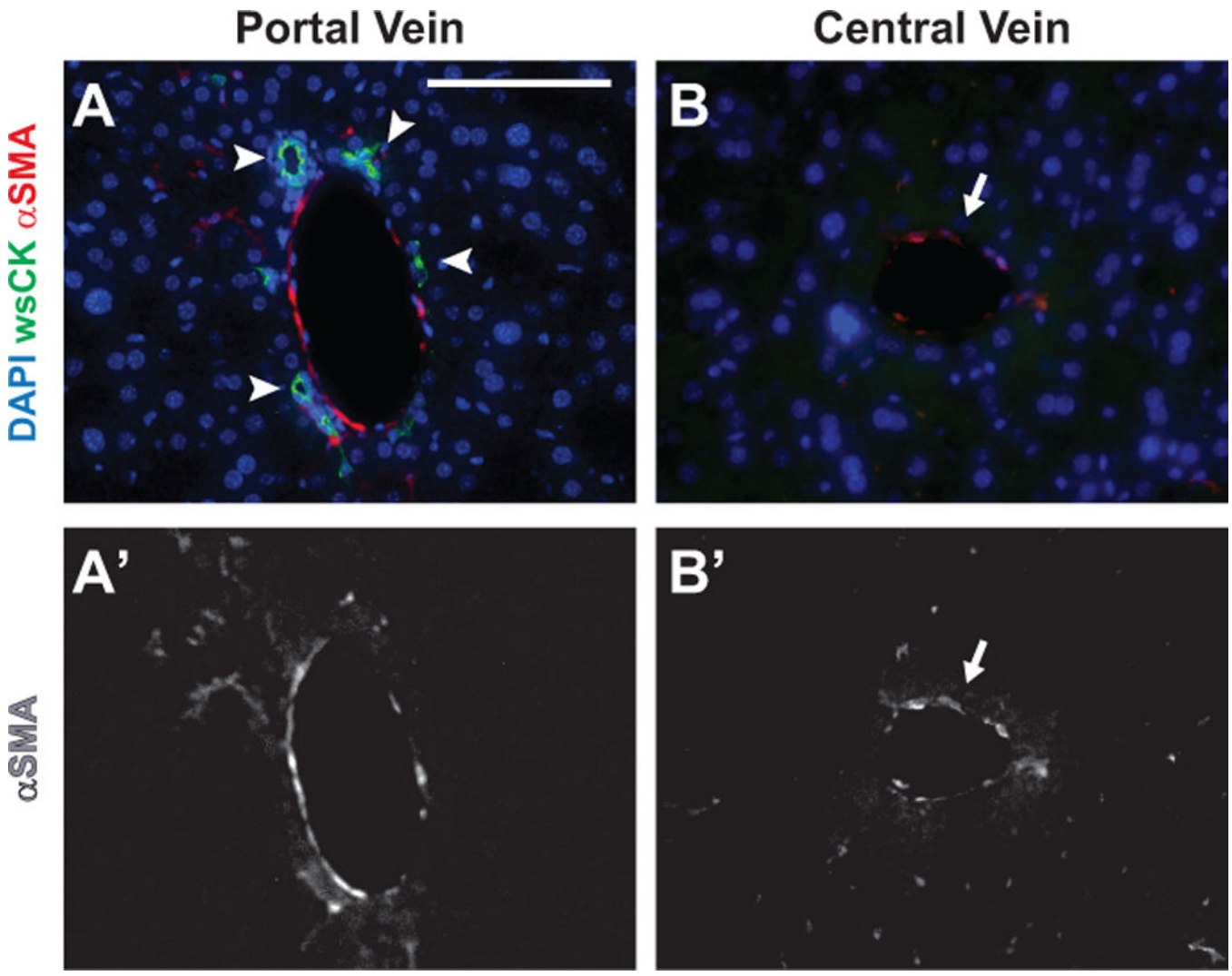

Figure 2. Distinguishing central veins from PVs.

(A). A PV is identified by the presence of αSMA staining and surrounding wsCK+ cholangiocytes (arrowheads). **(B).** Central veins are identified by the presence of αSMA staining with no wsCK+ cholangiocytes present around the structure (arrow). (**A' and B').** Grayscale images showing the αSMA channels from A and B, respectively. Scale bar in A is 100 μm and applies to all panels.

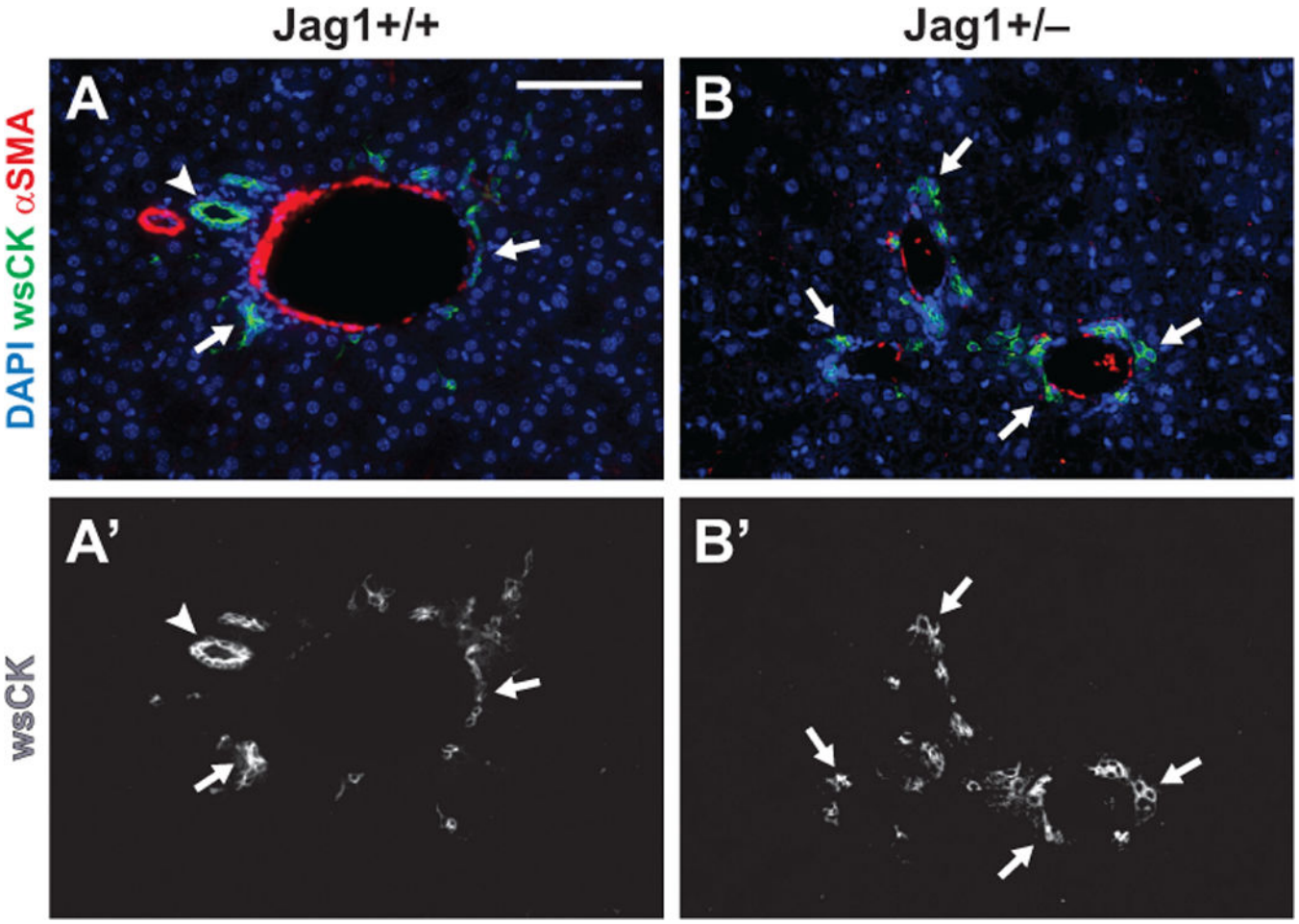

Figure 3. Identification of patent BDs.

(**A-A'**). In P30 wild-type livers, we count round to ellipsoid structures with a discernable lumen surrounded by wsCK+ cholangiocytes as a patent BD (arrowhead). Cholangiocytes which are not surrounding a lumen are considered unincorporated and are not counted (arrows). (**B-B'**). In *Jag1+/−* livers, cholangiocytes are still present (arrows). However, most are not incorporated into patent BDs. Scale bar in A is 100 μm and applies to all panels.

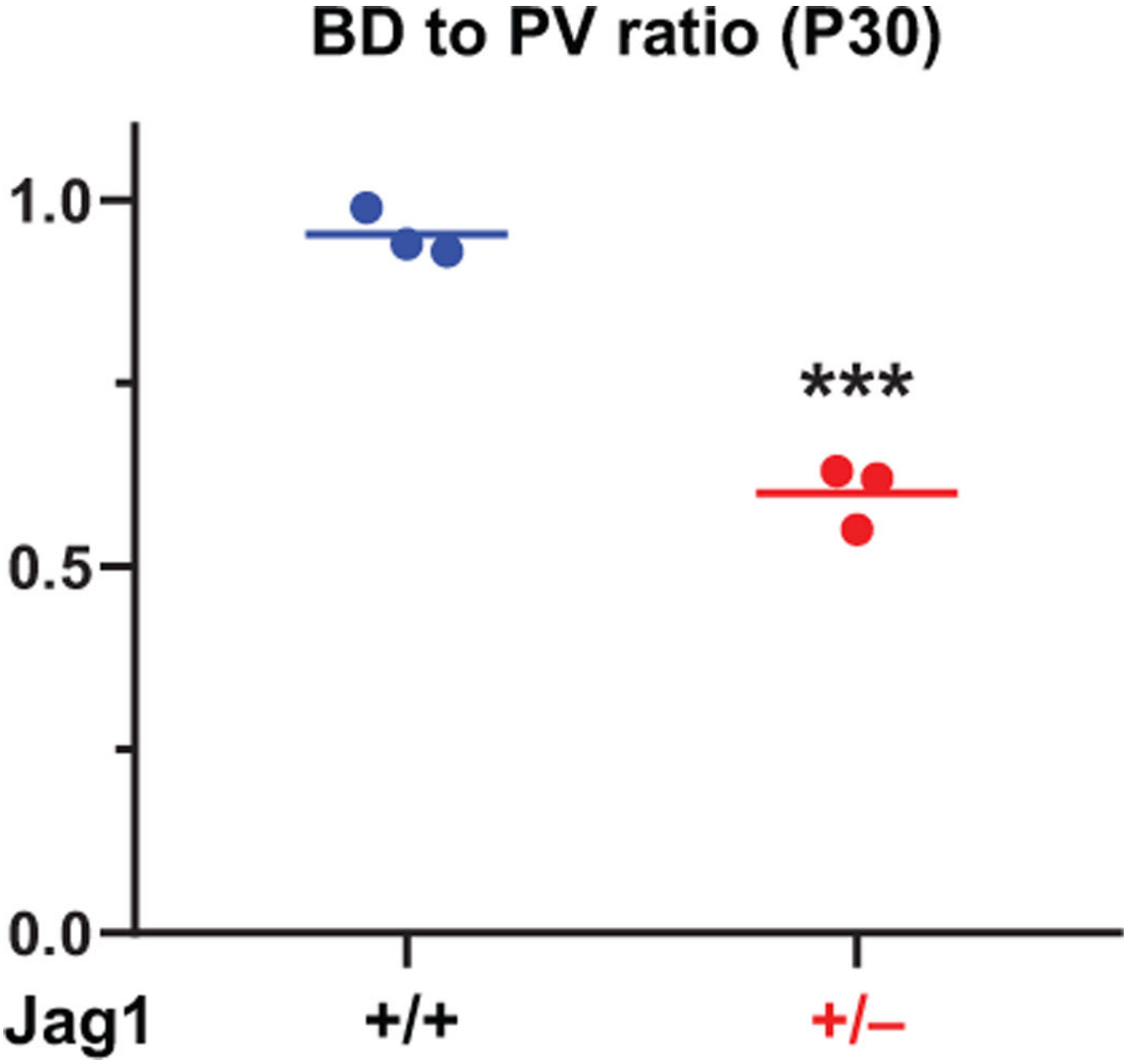

Figure 4. The BD to PV Graph from P30 mouse livers.

BDs and PVs are quantified and the BD to PV ratio is generated. As reported previously[8], *Jag1+/−* animals have a characteristic and significant decrease in BD to PV ratio compared to wild-type animals. For statistical analysis, two-way *t*-test was performed. Horizontal lines show means. *** $P<0.001$.

Table of material

Name of Material/ Equipment	Company	Catalog Number	Comments/Description
Isothesia (Isoflurane)	Henry Schein	11695–6776–2	
Desiccator	Bel-Art	16–800–552	
10% PFA	Electron Microscopy Sciences	15712	
50mL tube	ThermoScientific	339653	
70% Ethanol	Decon Laboratories	2401	
95% Ethanol	Decon Laboratories	2801	
100% Ethanol	Decon Laboratories	2701	
HistoChoice	VWR Life Sciences	H103–4L	
Omnisette Tissue Cassette	Fisher HealthCare	15–197–710E	
Macrosette	Simport	M512	
Paraplast X-TRA	McCormick Scientific	39503002	Parrafin
Tissue Mold	Fisher Scientific	62528–32	
Microtome	Microm	HM 325	
Superfrost Plus Microscope Slides	Fisher Scientific	12–550–15	
Xylene	Fisher Scientific	C8H10	
Tris-Based Antigen Retrieval	Vector Laboratories	H–3301	
Pressure Cooker	Instant Pot	Lux Mini	
Mini Pap Pen	Life Technologies	8877	
Polyoxyethylene 20 Sorbitan Monolaurate (Tween–20)	J.T. Baker	X251–07	
Octyl Phenol Ethoxylate (Triton-X–100)	J.T. Baker	X198–07	
Normal Goat Serum	Jackson Immunoresearch	005–000–121	
anti-CK8	Developmental Studies Hybridoma Bank	TROMA-I	Antibody Registry ID AB531826
anti-CK19	Developmental Studies Hybridoma Bank	TROMA-III	Antibody Registry ID AB2133570
anti-αSMA	Sigma Aldrich	A2547, Clone 1A4	
anti-rat-Alexa488	ThermoFisher	A21208	
anti-mouse-Cy5	Jackson Immunoresearch	715–175–151	
DAPI	Vector Laboratories	H-1000	
22×50 micro cover glass	VWR Life Sciences	48393 059	
Fluorescence Microscope	Leica	DMI6000 B	
Kimwipes	Kimtech Science	05511	